AJNR

Lhermitte-Duclos Disease: Assessment with MR Imaging, Positron Emission Tomography, Single-photon Emission CT, and MR Spectroscopy

Joachim Klisch, Freimut Juengling, Joachim Spreer, Donatus Koch, Torsten Thiel, Martin Büchert, Sebastian Arnold, Friedrich Feuerhake and Martin Schumacher

AJNR Am J Neuroradiol 2001, 22 (5) 824-830
http://www.ajnr.org/content/22/5/824

AJNR Am J Neuroradiol 22:824–830, May 2001

Case Report

Lhermitte-Duclos Disease: Assessment with MR Imaging, Positron Emission Tomography, Single-photon Emission CT, and MR Spectroscopy

Joachim Klisch, Freimut Juengling, Joachim Spreer, Donatus Koch, Torsten Thiel, Martin Büchert, Sebastian Arnold, Friedrich Feuerhake, and Martin Schumacher

Summary: Lhermitte-Duclos disease (LDD) is a rare cerebellar lesion with features of both malformation and benign neoplasm. However, the fundamental nature of the entity, its pathogenesis, and the exact genetic alterations remain unknown. We describe MR findings (including perfusion- and diffusion-weighted images) in two patients with LDD, as well as findings from single-photon emission CT (SPECT), MR spectroscopy (MRS), and fluorodeoxyglucose (FDG) positron emission tomography (PET) that give additional information about tumor pathophysiology. MR imaging usually distinguishes the LDD by its characteristic "tiger-striped" appearance. The regions of increased regional cerebral blood volume (rCBV) within the lesion correlated closely to the regions of FDG-hypermetabolism and high thallium (201-Tl) uptake. Proton MRS revealed an increased level of lactate and decreased level of myo-inositiol and *N*-acetyl-aspartate, as observed in low-grade gliomas, but decreased levels of choline. Our cases indicate that the functional investigations give additional information about tumor pathophysiology and reflect the histopathologic controversial entity with both characteristics found in low-grade gliomas and characteristics not typical for tumors.

In 1920, Lhermitte and Duclos described a rare dysplastic gangliocytoma (Lhermitte-Duclos disease). The nature of LDD and its pathogenesis, as well as the exact genetic alterations, are unknown. In view of the debate whether LDD represents a neoplastic, malformative, or harmartomatous lesion, we examined two patients by use of different imaging techniques.

Case Reports

Case 1

A 49-year-old woman had a 2-year history of progressive weakness of the limbs, progressive occipital headache, and blurred vision. Neurologic examination revealed a mild dysmetria and dysdiadochokinesia on the right, with imbalance. Mild, bilateral papilledema was present. As an adolescent, she had a strumectomy; on relapse, trichilemmomas were observed. At age 46 years, a basalioma was excised from her nose. CT scanning exhibited a partially calcified mass with corresponding susceptibility artifacts on T2*-weighted images in the right cerebellar hemisphere on MR images. The mass led to compression of the fourth ventricle and cerebral aqueduct with an obstructive hydrocephalus. Imaging findings strongly indicated LDD. The patient underwent surgery with partial removal of the lesion. Pathohistologic examination confirmed LDD [World Health Organization (WHO) grade I], with a relatively high density of small vessels within the lesion and no signs of proliferation (Fig 1C). No progression of the residual tumor was revealed by follow-up MR imaging 1 year after surgery; the hydrocephalus was found to be regredient (Fig 1A). MR imaging of the brain showed a residual, non-enhancing mass in the right cerebellar hemisphere. There was the aspect of two tumor components: a small, solid component located eccentric to the second one, characterized by a striated pattern of hyperintensity on T2-weighted images and corresponding hypointensity on T1-weighted images (Fig 1A). There was bright signal within the mass on diffusion-weighted images, whereas apparent diffusion coefficent (ADC) mapping revealed no disturbance of diffusion (Fig 1B). The resection margin of the tumor was seen on ADC maps. Detailed scanning with 1-mm multiplanar reconstructions of the multiplanar reconstruction sequence revealed a periventricular nodular heterotopia (PNH) in the subependymal white matter above the caudate nucleus of the left hemisphere (Fig 1A). Perfusion-weighted imaging of the tumor showed elevated regional cerebral blood volume (rCBV) and regional cerebral blood flow (rCBF) (Fig 2A) with an asymmetry index (relative values) of rCBV (right 49.1/left 25.4), rCBF (right 16.4/left 8.1), and mean transit time (right 3.1/left 3.2). Two single-photon emission CT (SPECT) scans were obtained, with no abnormal uptake on the early scan. Another scan obtained after 2 hours indicated a moderate increase in thallium (TI) uptake with a tumor-to-normal brain ratio of 1:2 (Fig 2B). Fluorodeoxyglucose (FDG) positron emission tomography (PET) showed a hypermetabolism of the LDD (Fig 2C). The asymmetry index of tumor 18-FDG uptake was 41%. The region of increased rCBV within the lesion correlated closely to the regions of FDG hypermetabolism and 201-TI uptake. Proton (^{1}H) MR spectroscopy (MRS) showed an elevated level of lactate with decreased levels of myo-inositol, *N*-acetylaspartate (NAA), creatine, phosphocreatine (Cr), and choline-containing compounds (Cho). Figure 3 summarizes the results of automated quantitative analysis. Further screening for cancers revealed an occult breast cancer. The diagnosis of Cowden's syndrome (CS) was assumed. Molecular analysis confirmed the suspected diagnosis. Sequencing of exon 9 revealed a base exchange A-G in the highly conserved position 2 of the splice acceptor site (c.1027–2A-G) (1). For a presymptomatic diagnosis, PTEN germline mutation analysis

Received August 2, 2000; accepted October 16.

From the Departments of Neuroradiology (J.K., J.S., S.A., M.S.), Nuclear Medicine (F.J.), and Stereotactic Neurosurgery (D.K.), and the Section of Medical Physics, Department of Radiology (T.T., M.B.), and the Department of Neuropathology (F.F.), University of Freiburg, Freiburg, Germany.

Address reprint requests to Joachim Klisch, Department of Neuroradiology, University of Freiburg, Breisacher Str. 64, D-79106 Freiburg, Germany.

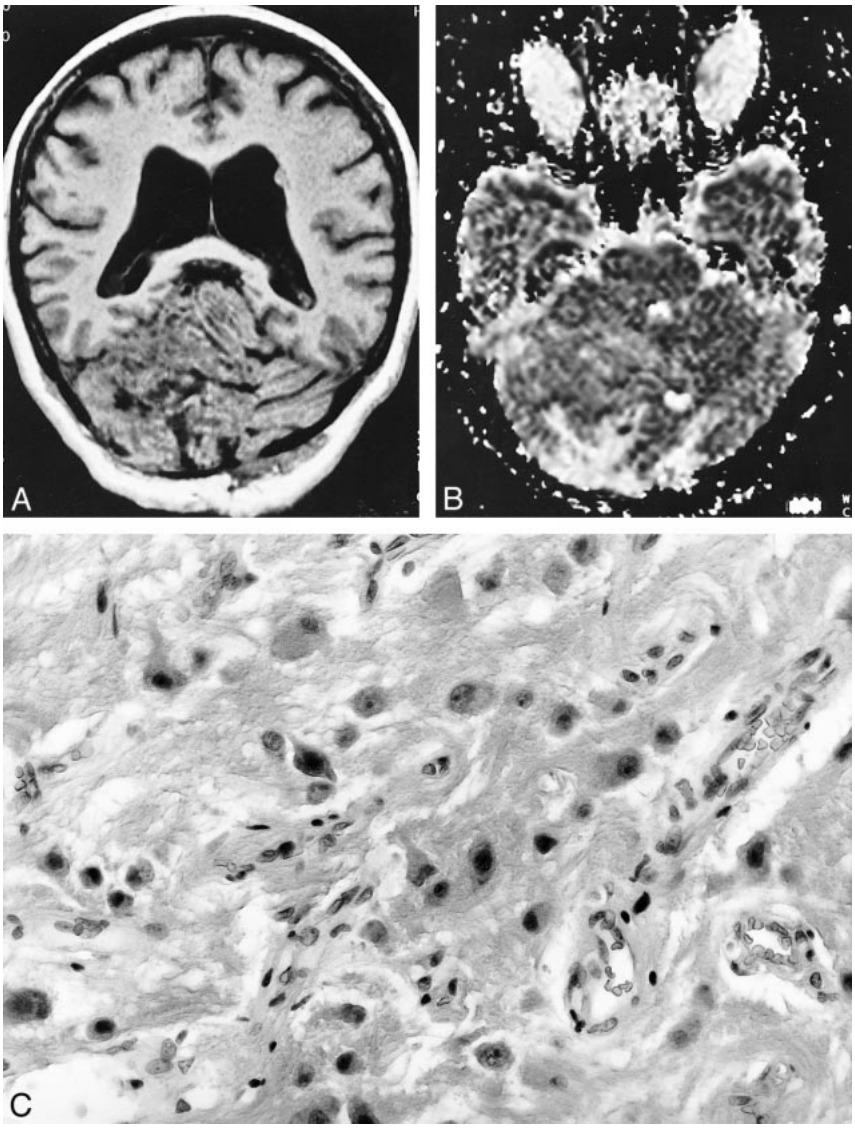

FIG 1. *A,* Coronal multiplanar reconstruction (MPR) of the MPR sequence (9.7/4/12/160/1 [TR/TE/flip angle/partitions/slice thickness in mm]), control 1 year after surgery, showing regredient hydrocephalus and solid and more ''tiger-striped'' components of the mass. Note periventricular nodular heterotopia. A 1.5-T scanner (Magnetom Vision; Siemens, Erlangen, Germany) with a standard gradient system (25mT/m, 600 μs risetime) and a circular polarized head coil was used.

B, Apparent diffusion coefficient (ADC) map of the Lhermitte-Duclos disease (LDD) after surgery shows no disturbance of diffusion within the lesion. The resection margin is detectable. High-speed multislice diffusion imaging was performed using echo-planar diffusion-weighted imaging (0.8/123 [TR/TE]) with b values of 50, 500, and 1000. ADC maps were calculated to quantify areas of low diffusion.

C, Histologic analysis of LDD (hematoxylin and eosin staining, magnification ×430) shows high density of small vessels within the lesion and dysplastic Purkinje cells.

was performed in her children by direct sequencing of all nine exons of PTEN.

Case 2

A 42-year-old man had a 6-week history of occipital headache. Neurologic examination revealed no focal neurologic deficits, and the headache was classified as migraine. CT scanning exhibited a non-calcified and non-enhancing hypodense mass in the left cerebellar hemisphere, with dislocation of the fourth ventricle. MR imaging of the brain showed a non-enhancing mass in the left cerebellar hemisphere. There was the aspect of two tumor components: a small solid component located excentric to the second one, characterized by a striated pattern of hyperintensity on T2-weighted images and corresponding hypointensity on T1-weighted images. The LDD-typical ''tiger-striped'' structure was best recognized on inversion-recovery–time (TIR) images. The abnormally thickened folia were characterized by strong signal intensity on diffusion-weighted imaging with a high b factor, whereas ADC mapping showed no pathologic signal disturbances. On T2*-weighted images (corresponding to CT scan) no significant susceptibility artifact was seen in the lesion (not shown). Tl-201 SPECT showed a significant elevated uptake of the tracer within the left cerebellar hemisphere, more pronounced within the solid component of the LDD (tumor-to-normal brain ratio of 1.3). This uptake was distributed over almost the whole cerebellar hemisphere and clearly visible on the early scan. FDG-PET revealed increased 18-FDG accumulation within the whole left cerebellar lesion, but markedly in the solid component of the tumor. The asymmetry index of tumor 18-FDG uptake was 37%. The region of increased rCBV, as demonstrated by xenon CT, correlated closely to the regions of FDG hypermetabolism and high 201-Tl uptake. ^{1}H MRS showed an elevated level of lactate with decreased levels of myo-inositol, NAA, and Cho (Fig 3).

MR diagnosis of LDD was feasible. Control MR imaging was performed over a period of 2 years and no changes in extension or configuration of the LDD was seen on standard sequences, including diffusion-weighted images. No clinical signs of CS were detected, and no LDD or CS in members of the patient's family were found. Genetic screening was impossible, because the patient refused to be tested.

Discussion

The clinical course in our cases is in accordance with other published cases of LDD (2, 3). LDD is classified as WHO grade I (4), but has the propensity to progress or to recur after surgery. Although rare associations between LDD and other brain tu-

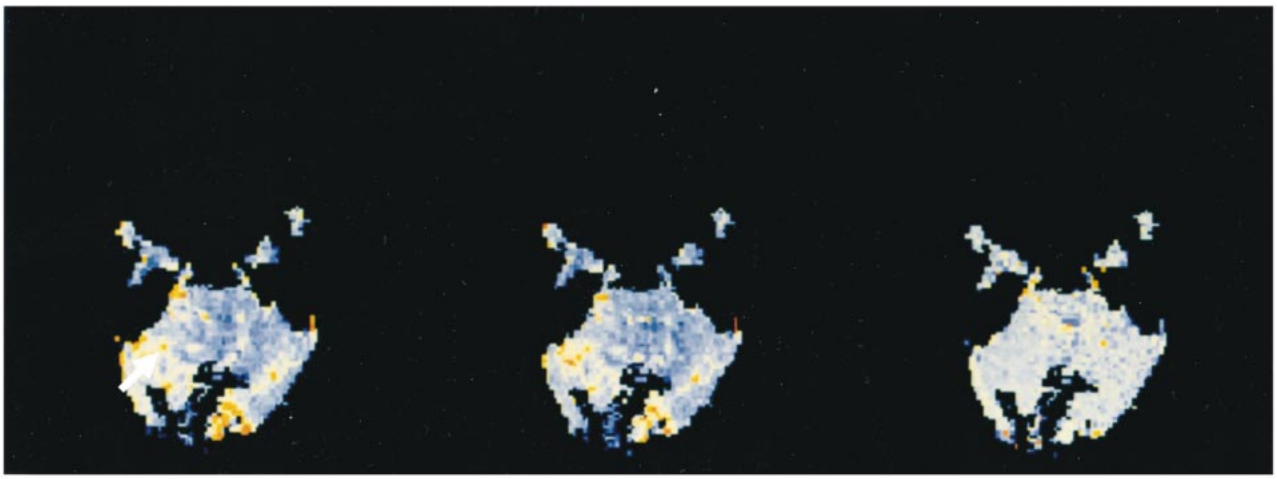

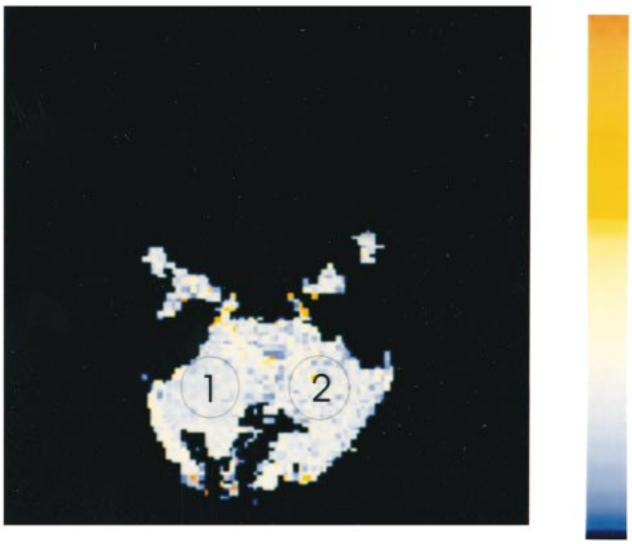

	rCBV (rel.values)		rCBF (rel.values)		MTT (rel.values)	
	mean	std	mean	std	mean	std
ROI 1	49,1	21,3	16,4	8,8	3,1	0,4
ROI 2	25,4	14,2	8,1	4,1	3,2	0,8

A

FIG 2. *A* (above), Perfusion MR shows marked increase of regional cerebral blood volume (rCBV) and regional cerebral blood flow (rCBF) within the solid component of the lesion (*arrow*). Note that there is no interhemispheric difference in mean transit time (MTT). A total of 12 mL of gadopentate dimeglumine was administered (4 mL/s) and a T2*-weighted gradient-echo sequence with multishot echo-planar sequences 0.8/10/90 (TR/TE/flip angle) was obtained, followed by image postprocessing with maps of rCBV, MTT, rCBF, and time to peak.

B (facing page), Single-photon emission CT images obtained 120 minutes after administration of 94 MBq 201-thallium (TI) shows ncreased 201-TI uptake within the solid part of the residual LDD (*arrow*). This area corresponds to the zone of increased rCBV and rCBF shown in *A*. Images were aquired with a rotating gamma camera (Siemens ZLC 370/750, Germany) 5 minutes and 120 minutes after intravenous administration of 97 MBq 201-TI. Data acquisition was completed after 32 minutes by using a 128 × 128 matrix. Butterworth and Ramp filters were used to reconstruct images. Ratios of regions of interest compared with contralateral cerebellum were calculated.

C (facing page), 18-FDG-PET with 3D MR imaging overlay shows the increased 18-FDG uptake is within the solid component of the LDD (*arrow*) and corresponds to the zone of increased rCBV and increased 201-TI uptake (see *A* and *B*). A Siemens CTI ECAT EXACT tomograph scanner (Germany) was used with a 10.8-cm field of veiw and 6.8-mm full width half maximum. The images were acquired 30 minutes after injection of 185 MBq 18-FDG. Images with attenuation correction were reconstructed using the standard mathematical algorithm implemented in ECAT software and using filtered back-projection by Shepp-Logan filter (cut-off 0.35 cycles/pixel). Automated spatial normalization to the stereotactic Talairach space was performed using SPM96. ROIs confined to the LDD were defined in all realigned slices covering the mass lesion, and identical regions were defined for the contralateral unaffected cerebellar hemisphere. Mean values for semiquantitative analysis of each region of interest (ECAT counts per pixel per second) were normalized to individual global brain glucose metabolism to give a glucose metabolic index as region of interest over global cerebral metabolic rate of glucose.

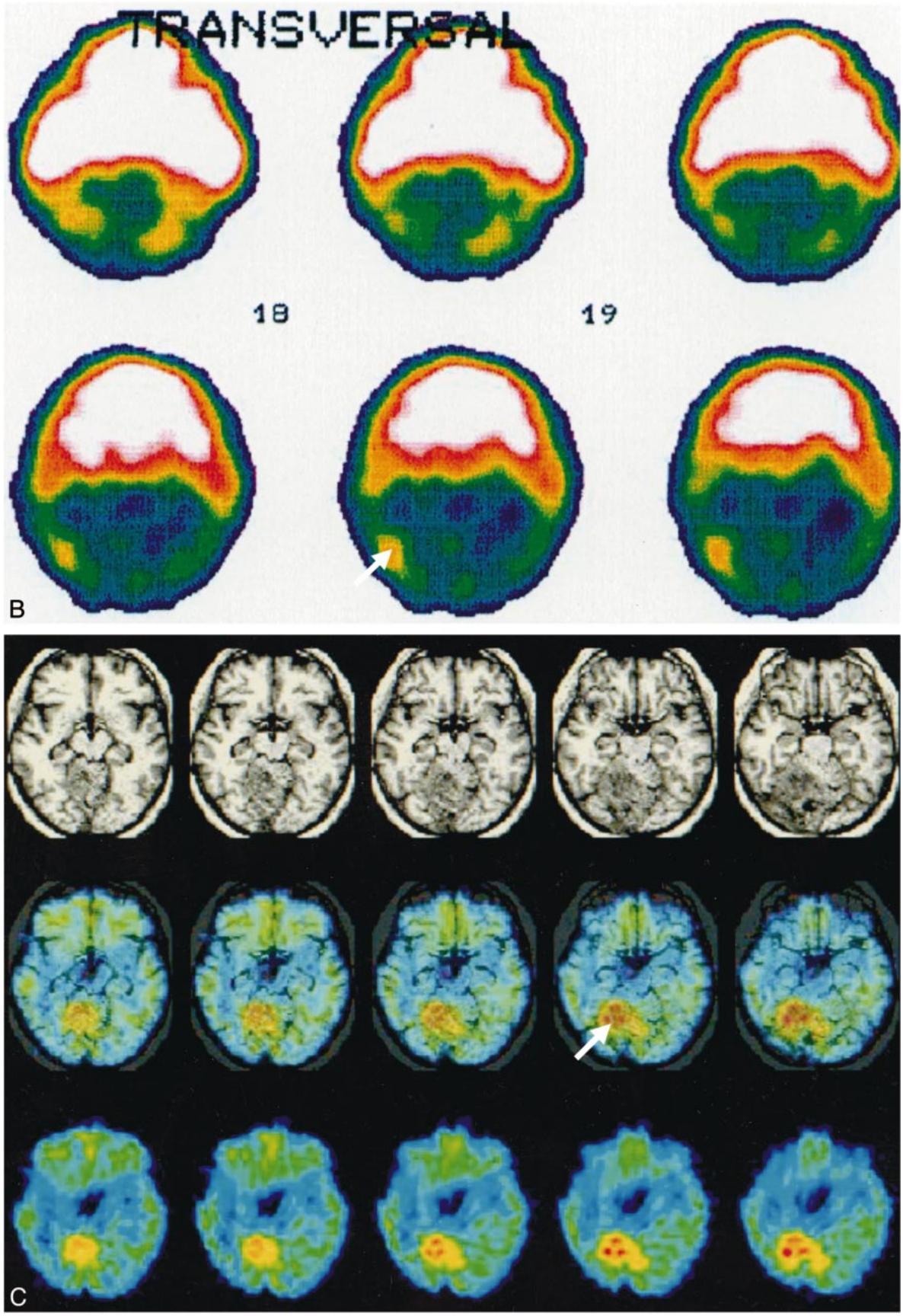

FIG 2. Continued.

									Difference in % to Control from Lit.14					
Patient Control	Case	Cr*	Glu*	Ins*	Lac*	NAA+ NAAG *	GPC +PCh bzw. Cho	NAA/(Cr +Cho)	Cr	Glu	Ins	Lac	NAA +NA AG	Cho
P	Case 1 right	1.00	1.495	0.191	1.472	1.014	0.137	0.89	0		-76	+++	-19	-51.1
P C	Case 1 left	1.00	0.982	0.576		1.135	0.214	0.93	0		-28		-9.2	-23.6
P	Case 2 left	1.00		0.58	1.30	1.16	0.14	1.02	0		-28	+++	-7.2	-50
P	P from Lit.14	1.00		0.14		1.10	0.21	0.91	0		-83		-12	-25
C	Control	1.00	1.527	0.751		1.171	0.286	0.91	0		-6		-6.3	2.143
C	Control from Lit.14	1.00		0.80		1.25	0.28	0.98	0		0		0	0

*Concentrations related to Creatin

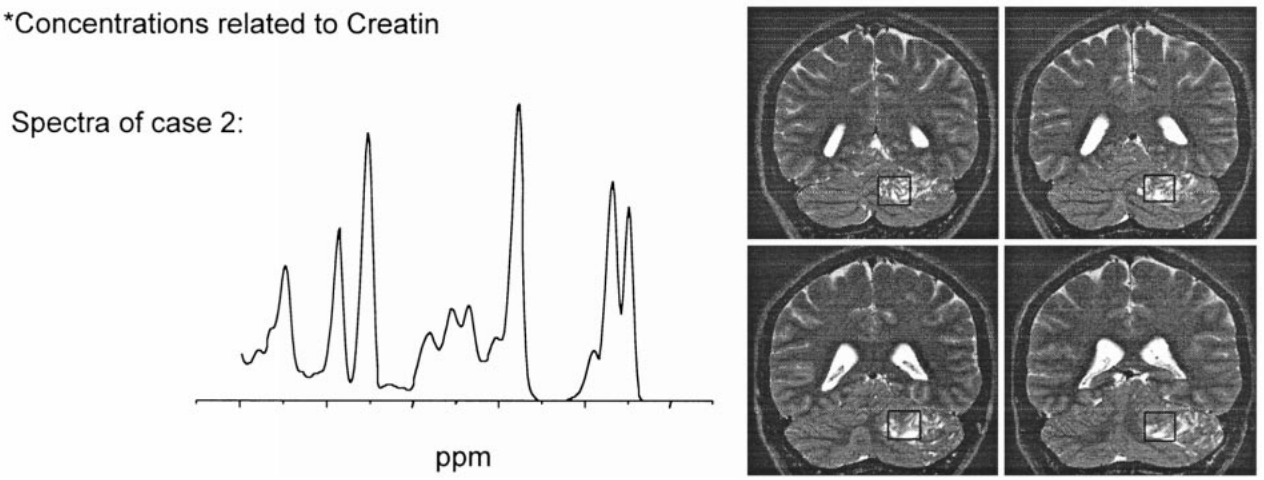

FIG 3. (Case 1 and 2). MR spectroscopy shows increased lactate levels and reduced levels of choline and myo-inositol. For comparison, we added the data from Verheggen's patient (14). ^{1}H MR spectra 1.5-T whole-body system (Sonata; Siemens, Erlangen, Germany) or 2-T whole-body system (Medsped S200 Avance; Bruker, Karlsruhe, Germany) with a gradient insert of 30mT/m stength and 190 ms ramp time were localized with a point-resolved spectroscopy select sequence (3000/30 or 128/88 or 20mm^3 [TR/TE/repetitions/volume of interest]). A water suppression preparation period using three optimized chemical shift selective cycles was applied before each measurement. For each localization, a reference scan without water suppression was acquired. Spectra were analyzed using the LCModel software with the appropriate reference spectra.

mors have been reported (5, 6), until now, an association between LDD in CS with PNH as found in case 1 has never been described. PNH represents either clusters of neurons demonstrating an arrested migration, or a failure of genetically determined cell death in collections of neuroblasts within the periventricular germinal matrix (7). In the migratory disorder of tuberous sclerosis, PNH is a prominent component, but may also occur as an isolated defect in otherwise normal brains (8). CS, with its several neurologic and cutaneous symptoms, shares features with other phakomatoses, eg, tuberous sclerosis. Sequencing of exon 9 revealed a base exchange A-G in the highly conserved position 2 of the splice acceptor site, a new kind of mutation that has been never described before in CS (1).

Conventional MR findings and the possible differential diagnoses in our cases are in accordance with other published cases of LDD (2, 3). A nonenhancing mass in the posterior fossa with unilateral hemispheric expansion, hypointense on T1-weighted images and hyperintense on T2-weighted images, with parallel linear striations on the surface of the lesion, should be considered specific for LDD in a middle-aged adult. The morphologic features of the LDD could be demonstrated most clearly with the TIR sequence and the turbo inversion-recovery magnitude (TIRM) sequence. Areas of calcifications, as found in case 1, could be equally well depicted on T2*-weighted images; therefore, a CT scan is not necessary.

Owing to the T2 effect, the abnormally thickened folia in the LDD were characterized by slightly higher signal intensities on diffusion-weighted images with low b factors than with high b factors, whereas ADC mapping showed no disturbance of water diffusion. The signal on diffusion-weighted images and ADC maps depends on cell density, low extracellular water content, and enhancement of the tumor (9). Profusion of dysplastic cortical neurons in LDD, a thickening of the molecular layer, the loss of Purkinje cells, and thinning of medullary white matter may be responsible for findings on diffusion-weighted images. Comparable to the TIRM sequence, diffusion-weighted imaging, especially ADC mapping, is helpful in postoperative

control because it delineates tumor from surgical resection margins, whereas on T2-weighted images, differentiation between both components seems to be more difficult (see case 1).

Contrast enhancement is not a typical sign of LDD (10). If contrast enhancement is present, other diagnoses, such as (capillary) hemangioblastoma, might be suggested. Hemangioblastomas commonly have enlarged vessels, solid and cystic components, and no striations. There was no contrast enhancement in our cases on MR images, whereas perfusion-weighted imaging in case 1 and xenon CT in case 2 showed increased rCBV and rCBF within the lesion. Siegal et al (11) used relative CBV mapping for routine evaluation of patients with different brain tumors and assumed that regional CBV mapping correlates with active tumor components. We assume that hyperperfusion without enhancement correlates closely to the histopathologic observation of numerous dilated thin-walled blood vessels (9) and generalized proliferation of blood vessels within LDD (4) (Fig 1C). Proliferation of blood vessels per se is not a sign of malignancy. These histologic findings are comparable to some pilozytic astrocytomas or vascularized meningiomas that are WHO grade I (4), but these tumors show contrast enhancement.

In the examination of intracranial tumors, 201-Tl SPECT may help to differentiate between malignant (high uptake) and benign gliomas (low uptake) (13). Tl-201 is a potassium analogue, and its uptake by tumors is thought to reflect regional blood flow, a defective blood-brain barrier, and cellular uptake via Na^+-K^+adenosine triphosphatase (ATPase) on the cell membrane. High uptake of 201-Tl also occurs in hypervascular benign tumors, such as meningiomas. In our cases, LDD showed significant uptake of 201-Tl on SPECT scans in relation to histopathologic findings and to perfusion measurements owing to regional increased blood flow rather than dysfunction of ATPase in the diffuse, cortical, accumulated, abnormally large, dysplastic granular cells. Therefore, our findings of high uptake on 201-Tl SPECT scans are in accordance with findings in other low-grade vascularized tumors of the brain (13).

High FDG uptake, usually indicating malignancy, is misleading in the presented cases. Whether the increased 18-FDG accumulation within the lesion is due to increased overall cell metabolism or reflects an isolated upregulation in enzyme activity of hexokinase remains unclear. In light of histopathologic findings in LDD, characterizing the lesions as hamartomatous overgrowth with double-layered structures comprising a layer with increased density of dysplastic granular cells, the increased 18-FDG uptake may simply reflect the focally increased cell density and/or a different glucose metabolism of these dysplastic cells.

LDD has some characteristics of tumors, such as decreased NAA and increased lactate, but not increased levels of lipids. On the other hand, decreased Cho/Cr (and myo-inositol/Cr) ratios are in strict contrast to observations in cerebral tumors, where increases of Cho (and myo-inositol) levels are associated with enhanced membrane turnover and demyelination. Verheggen et al (14) showed a decreased Cho/Cr ratio in one case of a bilateral LDD (Fig 3) and concluded that this finding was in strict contrast to observations in cerebral tumors. Lactate, normally undetectable in brain, accumulates in cysts, necrotic tissue, or within active tumors because of the high rate of glycolysis (glucose to lactate) within tumors of all types, including aerobic tumors. Together with the hypermetabolism found in FDG-PET, we assume that the elevated lactate level is due to an abnormal high glucose metabolism (glycolysis) within the LDD, rather than representing high lactate levels in cystic or necrotic components of LDD. Furthermore, in one case of LDD, we found an elevated level of alanine, an alternative reduced partner of pyruvate derived from glycolysis. The normal level of lipids and the histopathologic findings of no necrotic areas within the LDD support our thesis that elevated lactate levels do not represent cell death. Therefore, our results of MRS in LDD are, in part, in contrast to those reported by Verheggen et al (14), which showed no changes in lactate levels (Fig 3).

Conclusion

Although the exact pathophysiologic explanation for the signal characteristics of LDD in diffusion-weighted imaging/perfusion-weighted imaging, ^{1}H MRS, FDG-PET, and 201-Tl SPECT remains unknown, our cases indicate that functional imaging of the LDD gives further information about the pathophysiology of this very rare entity. Our results of functional investigations on LDD reflect the histopathologic controversial entity. Because of the clinical question, whether to resect the LDD in cases of no mass effect, these functional examinations might give further information to predict the natural course of the tumor and might, therefore, influence the indication for surgery in the future.

References

1. Schnieders B, Burger B, Dichgans C, Müller K, Friedl W. **PTEN splice-site mutation in a patient with Cowden disease.** *Medgen* 2000;12:126
2. Kulkantrakorn K, Awwad EE, Levy B, et al. **MRI in Lhermitte-Duclos disease.** *Neurology* 1997;48:725–731
3. Meltzer CC, Smirniotopoulos JG, Jones RV. **The striated cerebellum: an MR imaging sign in Lhermitte-Duclos disease (dysplastic gangliocytoma).** *Radiology* 1995;194:699–703
4. Kleihues P, Cavenee W K, eds. ***Pathology and Genetics of Tumours of the Nervous System. WHO Classification of Tumours.*** Lyon: IARC Press; 2000:235–237
5. Lindboe CF, Helseth E, Myhr G. **Lhermitte-Duclos disease and giant meningioma as manifestations of Cowdens disease.** *Clin Neuropathol* 1995;14:327–330
6. Domingo Z, Fisher-Jeffes ND, deVilliers JC. **Malignant occipital astrocytoma in a patient with Lhermitte-Duclos disease (cerebellar dysplastic gangliocytoma).** *Br J Neurosurg* 1996;10:99–102
7. Raymond AA, Fish DR, Stevens JM, Sisodiya SM, Alsanjari N, Shorvon SD. **Subependymal heterotopia: a distinct neuronal**

migration disorder associated with epilepsy. *J Neurol Neurosurg Psychiatry* 1994;57:1195–1202
8. Huttenlocher PR, Taravath S, Mojtahedi S. **Periventricular heterotopia and epilepsy.** *Neurology* 1994;44:51–55
9. Klisch J, Husstedt H, Hennings S, von Velthoven V, Pagenstecher A, Schumacher M. **Supratentorial primitive neuroectodermal tumours: diffusion-weighted MRI.** *Neuroradiology* 2000;42:393–398
10. Awwad EE, Levy E, Martin DS, Merenda GO. **Atypical MR appearance of Lhermitte-Duclos disease with contrast enhancement.** *AJNR Am J Neuroradiol* 1995;16:1719–1720
11. Siegal T, Rubinstein R, Tzuk-Shina T, Gomori JM. **Utility of relative cerebral blood volume mapping derived from perfusion magnetic resonance imaging in the routine follow up of brain tumors.** *J Neurosurg* 1997;86:22–27
12. Stapleton SR, Wilkins PR, Bell BA. **Recurrent dysplatic gangliocytoma (Lhermitte-Duclos disease) presenting with subarachnoid haemorrhage.** *Br J Neurosurg* 1992;6:153–156
13. Black KL, Hawkins RA, Kim KT, et al. **Use of thallium-201 SPECT to quantitate malignancy grade of gliomas.** *J Neurosurg* 1989;71:342–346
14. Verheggen R, Bruhn H, Schröder BU, Frahm J, Markakis E. **Lhermitte-Duclos disease: a critical appraisal of different radiologic methods.** *Eur J Radiol* 1994;19:21–24